

ORIGINAL ARTICLE

Photorefractive response and real-time holographic application of a poly(4-(diphenylamino)benzyl acrylate)-based composite

Ha Ngoc Giang, Kenji Kinashi, Wataru Sakai and Naoto Tsutsumi

A photorefractive (PR) composite based on poly(4-(diphenylamino)benzyl acrylate) (PDAA) as a host photoconductive matrix is reported. The PR performance was investigated at three different wavelengths (532, 561, 594 nm), and an optimized operating wavelength of 532 nm was obtained. The PDAA composite had high sensitivity at 532 nm with a maximum diffraction efficiency of >80%, which was achieved at an applied electric field of $40 \text{ V } \mu\text{m}^{-1}$. An application with a hologram display system using the PR composite was demonstrated. A clear and updatable hologram of an object was successfully reconstructed in real time, even at a low applied electric field of $25 \text{ V } \mu\text{m}^{-1}$.

Polymer Journal (2014) 46, 59–66; doi:10.1038/pj.2013.68; published online 14 August 2013

Keywords: composite; hologram; photoconductive polymer; photorefractive effect; wavelength

INTRODUCTION

Photorefractive (PR) polymers and composites have attracted much attention because of their interesting applications, such as data storage, three-dimensional (3D) displays, image amplification and optical phase conjugation. The mechanism for a PR effect is a combination of several steps: (1) non-uniform material illumination through a laser interference pattern, (2) charge generation assisted by a sensitizer, and (3) charge redistribution, which induces the spatial modulation of the refractive index through nonlinear optical (NLO) effects. The most fascinating application of updatable holographic 3D displays has been demonstrated.¹ Many parameters, including materials and measurement conditions, need to be chosen to successfully utilize PR devices as hologram displays.

First, the PR polymer and composite have an essential role, and material design is an initial step for fabricating PR devices. The origin of the PR effect is based on the properties of the material used. Hence, material design must be carefully chosen to obtain suitable properties for a hologram display. Typical components of a PR composite include a photoconductive polymer, a NLO chromophore, a sensitizer and a plasticizer. The photoconductive polymer matrix provides the charge-transporting medium. The polymer serves as a dispersive matrix for other components. Thus, the photoconductive host polymer should possess high photoconductivity and an amorphous structure to ensure the optical clarity of the composite film. The most well-known photoconductive polymer, poly(*N*-vinylcarbazole) (PVK), has been widely used in PR research.^{2–7} However, PVK has disadvantages such as low hole mobility and a high glass transition

temperature (T_g) of >200 °C. Low hole mobility will limit the speed of space-charge field formation and consequently lead to a slow PR response time.

Another factor that will affect PR response time is the re-orientation of the chromophore, which has been shown to occur inside a low T_g composite and has an essential role in high PR performance.⁸ To decrease the T_g , a large amount of plasticizer and a small polymer concentration should be introduced into the composite.^{3,9} Other methods that can be applied to adjust T_g include using an internal plasticizer and elongating the alkyl chain that connects the photoconductive moiety and polymer main chain.¹⁰ However, both approaches must be carefully considered in terms of the photoconductive component dilution, which can lead to poor PR performance. Also, a high viscosity photoconductive matrix, which is one property of a high T_g polymer, creates additional difficulties when preparing PR devices. Fabricating a large-size PR device is more favorable for a hologram display compared with a typical measurement device ($30 \times 30 \text{ mm}^2$) and should be considered when the polymer matrix is chosen. However, the highest occupied molecular orbital (HOMO) of each PR component may directly affect the PR performance.

If a carbazole moiety is used as a photoconductor, it should be chosen carefully because of the relatively deep HOMO level (ionization potential = 5.9 eV). If the HOMO level of the charge-transporting manifold is lower than that of the chromophore, the PR performance may depend on the experimental details. This effect is called the preillumination effect and was described by Ostroverkhova.^{5,9}

Herlocker *et al.*¹¹ investigated a PR composite based on PVK, sensitizer C60 and a fluorinated styrene chromophore with various HOMO levels. An increase in the chromophore HOMO level led to response time stabilization, but it also accompanied a decrease in the PR dynamic range. Therefore, recent studies have focused on preparing the PR composite from a highly photoconductive polymer with a lower T_g and a lower HOMO level.

Polymers with the triphenylamine unit have received much attention for use in solar cells and organic light-emitting diodes because of their high photoconductivity.¹² As mentioned above, triphenylamine, which has a fast hole mobility (10^{-4} – 10^{-3} cm² V⁻¹ s⁻¹) and an appropriate HOMO level compared with carbazole, is a potential candidate as the next photoconductor for PR composites. Recently, polyacrylic tetraphenyldiaminophenyl (PATPD), a novel photoconductive polymer and copolymer based on TPD was synthesized and successfully applied to PR-based 3D displays.^{13–15} Using the new polymer matrix, a large-sized PR display device has been fabricated. A sub-millisecond response time was obtained using a composite based on PATPD and 2-(4-(azepan-1-yl)benzylidene)malononitrile (7-DCST) with assistance from a high applied field (95 V μm^{-1}) and a high-power and high-intensity pulsed laser.¹⁶ However, the complicated synthetic procedure for producing the PATPD photoconductive matrix may limit the usage of the new material due to its high cost. Tsujimura *et al.*¹⁷ investigated a PR composite based on poly(4-diphenylamino)styrene and applied this composite to a real-time hologram display. However, the study used small samples and a high intensity (3 W cm⁻²). A high applied electric field of ≥ 45 V μm^{-1} was needed for the PR characterization and the hologram display.

The following factors should be considered together when choosing a polymer matrix: ease of synthesis, appropriate T_g , ability to prepare a larger device, low operating laser intensity and low applied field. In this study, triphenylamine was used as a photoconductor. The acrylate was chosen to reduce T_g and provide a low viscosity, which are desirable properties for larger sample preparation. We synthesized poly(4-(diphenylamino)benzyl acrylate) (PDAA) using a simple synthetic procedure, and PDAA was used as the photoconductive matrix in the PR composites.

Second, the measurement conditions must be carefully considered to optimize the PR properties for a hologram display. The writing beam wavelength contributes significantly to the PR effect. Many studies have used a He-Ne laser (633 nm) for PR characterization because of its low absorption. However, increased charge generation in a stronger absorption region might improve the PR properties. Thus, the goal of optimizing the PR properties is to have a higher diffraction efficiency and a faster response time at a lower field. Here, PR performance was investigated using degenerated four-wave mixing and two-beam coupling with moderate-intensity lasers at different wavelengths (532, 561 and 594 nm). The most suitable wavelength was chosen for the hologram application. A hologram display system is demonstrated using the new composite with the simultaneous recording and reading of images at a low applied field.

MATERIALS AND METHODS

Device and material preparation

The PDAA polymer was used as the host photoconductive matrix. Also, 7-DCST was used as the NLO chromophore, and phenyl-C61-butyric acid methyl ester (PCBM) was used as the sensitizer. The plasticizer, benzyl *n*-butyl phthalate (BBP), was added to reduce T_g . The chemical structures of PDAA, 7-DCST, BBP and PCBM are shown in Figure 1. PDAA and 7-DCST were synthesized (see the Supplementary Information). The PDAA synthetic route is

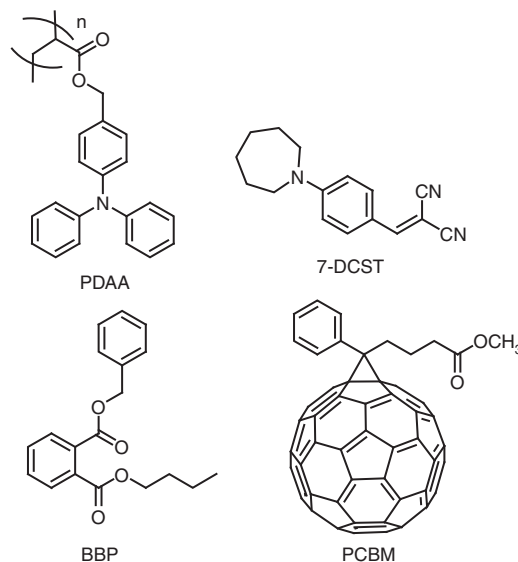


Figure 1 Chemical structures of PDAA, 7-DCST, BBP and PCBM.

shown in Scheme S1. The synthetic procedure for the PDAA monomer was performed according to previous reports.^{18,19} BBP was purchased from the Tokyo Kasei Kogyo Co., Tokyo, Japan. PCBM was purchased from Sigma-Aldrich Co., St Louis, MO, USA. Unless otherwise stated, all other chemicals were purchased from Wako Pure Chemicals Industries Ltd., Osaka, Japan.

All components, including PDAA, 7-DCST, BBP and PCBM, were mixed in tetrahydrofuran and stirred for 24 h. The composite has a composition of PDAA/7-DCST/BBP/PCBM = 55/40/4/1 weight percent. The mixture was then cast on a hot plate at 70 °C for 24 h, followed by drying in a vacuum oven at 60 °C for 24 h. The obtained composite was sandwiched between indium-tin-oxide plates at 130 °C. The composite film thickness was adjusted using Teflon spacers.

PR characterization

The diffraction efficiency of the PR sample was measured using a degenerate four-wave mixing (DFWM) technique. Varieties of cobalt semiconductor (25 mW) laser sources were used at different wavelengths of $\lambda = 532$, 561 and 594 nm, with a total incident intensity of 172, 174 and 216 mW cm⁻², respectively. The holographic gratings were written on the sample by two *s*-polarized beams that intersected at the sample position with incidence angles of 40° and 55° in air. A weak intensity *p*-polarized reading (probe) beam that was from the same source and counter-propagating to one of the writing beams was diffracted by the refractive index grating in the sample film. The diffracted signal propagated in the direction opposite to another writing beam and was reflected by a beam splitter. The diffracted signal was detected by a photodiode detector. The probe beam that transmitted through the sample film was also detected by another photodiode detector. From the transmitted beam intensity (I_t) and the diffracted beam (I_d), the diffraction efficiency (η) was calculated using equation (1):

$$\eta \% = \frac{I_d}{I_t + I_d} \times 100 \quad (1)$$

The PR response time was measured using the same geometry. The diffraction efficiency growth was fitted with a stretched exponential function using Kohlrausch–Williams–Watts (KWW) equation (2):

$$\eta = \eta_0 [1 - \exp(-t/\tau)^\beta], \quad (2)$$

where τ is the response time and β ($0 < \beta \leq 1$) is the fitting parameter related to the time width constant distribution.

The PR optical sample gain was measured using a two-beam coupling (TBC) technique. The same geometric configuration that uses two *p*-polarized beams of equal intensity that cross at the thin film sample, similar to the

DFWM technique, was used, except without a probe beam. The intensities of the two beams that transmitted through the sample film were measured using photodiode detectors to evaluate the optical gain using equation (3):

$$\Gamma = \frac{1}{d} (\cos \theta_A \cdot \ln \frac{I_A(I_B \neq 0)}{I_A(I_B = 0)} - \cos \theta_B \cdot \ln \frac{I_B(I_A \neq 0)}{I_B(I_A = 0)}), \quad (3)$$

where d is the sample film thickness, θ_A and θ_B are the internal angles of the two beams with respect to the normal direction and I_A and I_B are the intensities of the two beams after the sample film.

RESULTS AND DISCUSSION

A PDAA polymer with a molecular weight (M_w) of 11 000 and a polydispersity that is < 2 (1.86, see Supplementary Information) was obtained using a simple synthetic route. The synthesized PDAA exhibited a relatively low T_g (75 °C). This is one advantage of PR composites that are based on PDAA. Despite keeping the polymer concentration high (55% by wt.) and doping only a small amount of the plasticizer, BBP (4% by wt.), the T_g of the composite was reduced to room temperature (25 °C), which is suitable for chromophore orientation. With a NLO chromophore concentration of 40% and without additionally diluting the polymer concentration, which could lead to a lower photoconductivity, the appropriate T_g was obtained. By using a low viscosity polymer matrix of PDAA, large PR samples could be fabricated.

Figure 2 shows PR composite devices with various sizes. Sample (a) is the largest device (diameter = 8 cm) for use in the hologram movie, and sample (b) is a middle-sized device for use in the hologram display. Sample (c) is the test piece that measures fundamental PR responses, including diffraction efficiency, optical gain and response time. All three samples in Figure 2 were prepared using a simple gentle pressing method after the composite was melted at a temperature of 130 °C. No special equipment or high pressure is necessary for preparing these samples, which maintained their optical clarity for a few weeks at room temperature. By being stored in a refrigerator at 5 °C, the samples' stability was preserved for months. However, by increasing the temperature to 60 °C, the PR samples underwent chromophore recrystallization after only a few days. At

this stage, long-time stabilization had not been optimized. Many methods that use a different chromophore or a mixture of different chromophores and a monolithic polymer have been developed.^{20–22} A co-polymer containing triphenylamine and a small amount of the NLO chromophore in the polymer side chain will improve the compatibility between the matrix and the chromophore without reducing the polymer photoconductivity. Future work will focus on co-polymer synthesis to extend the shelf life while maintaining high PR performance.

In addition to material design, the writing beam wavelength should be carefully considered because the PR performance and holographic properties vary according to the absorption coefficient. Investigating the PR properties, such as a changing wavelength, may be important for optimizing the PR properties. To determine a suitable wavelength for the hologram application, we studied the PR effect on our composite using three operating wavelengths: 532, 561, and 594 nm. The diffraction efficiency results from the DFWM measurement were plotted as a function of the applied electric field, as shown in Figure 3a. High diffraction efficiencies were achieved at all the operating laser wavelengths with a moderate applied electric field. Upon 532 nm illumination, a maximum diffraction efficiency of $> 80\%$ was achieved at an applied electric field of $40 \text{ V } \mu\text{m}^{-1}$. The sinusoidal dependence of the diffraction efficiency as a function of the electric field could be explained using Kogelnik's coupled-wave theory.²³ The diffraction efficiency (η) is expressed as a function of refractive index modulation as follows:

$$\eta = \sin^2(K\Delta n \cos(\theta_B - \theta_A)), \quad (4)$$

where $K = \frac{\pi d}{\lambda(\cos\theta_A \cos\theta_B)^{1/2}}$; d is the film thickness, λ is the laser beam wavelength, θ_A and θ_B are the internal angles of the two beams with respect to the normal direction and Δn is the refractive index modulation. The value of Δn is the sum of the orientational birefringence and the electro-optic contribution, which strongly depends on the electric field in the PR polymer composite.⁸ As the external field increases, the internal space-charge field that is induced between the dark and bright areas inside the sample increases and is

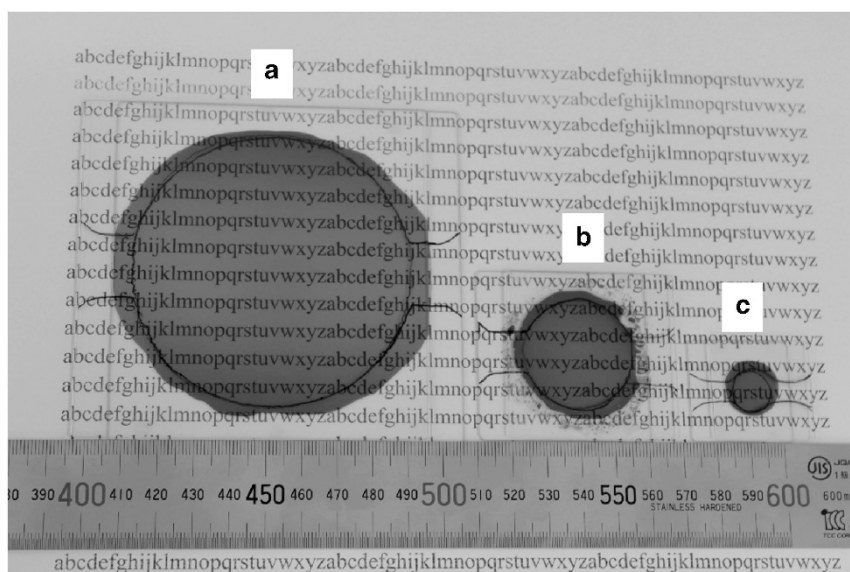


Figure 2 PR samples of different sizes. (a) A large-sized device with a diameter of 8 cm for a hologram movie. (b) A middle-sized device for a hologram display. (c) A test piece for measuring the basic PR quantities: diffraction efficiency, optical gain, and response time. A full color version of this figure is available at *Polymer Journal* online.

followed by an increasing Δn . The value of η follows the sine-squared function of Δn , and a diffraction efficiency peak appears near Δn of approximately 2×10^{-3} . The diffraction efficiency peak, as shown in Figure 3a, was shifted to a lower applied electric field when the shorter wavelength lasers were used. The diffraction efficiency change originated from changes in the refractive index modulation, Δn , as explained above. Thus, we suggest that the value of Δn varied when different operating wavelengths were used. Δn can be calculated using equation (4) with the η values from the DFWM results.

Figure 3b displays the calculated refractive index modulation values as a function of the applied electric field. At each specific applied electric field, the highest value of Δn was obtained with the shortest operating wavelength. This phenomenon could be due to the different absorption at each wavelength. The UV-visible absorption spectrum of the composite with a thickness of 100 μm is shown in Figure 4. The absorption spectrum is distributed broadly in the visible region, and the absorption coefficients increase with decreasing wavelength. The absorption growth observed in Figure 4 might contribute to the charge generation. Charge generation was supported by the photocurrent measurement, and the results are listed in Table 1. More charge carriers were produced at the shorter wavelengths. Subsequently, at a specific electric field, more charge carriers could migrate to dark areas and become trapped. As a result, a stronger space-charge field was formed at the lower electric fields, and a larger refractive index modulation was introduced. As shown in Figure 3b,

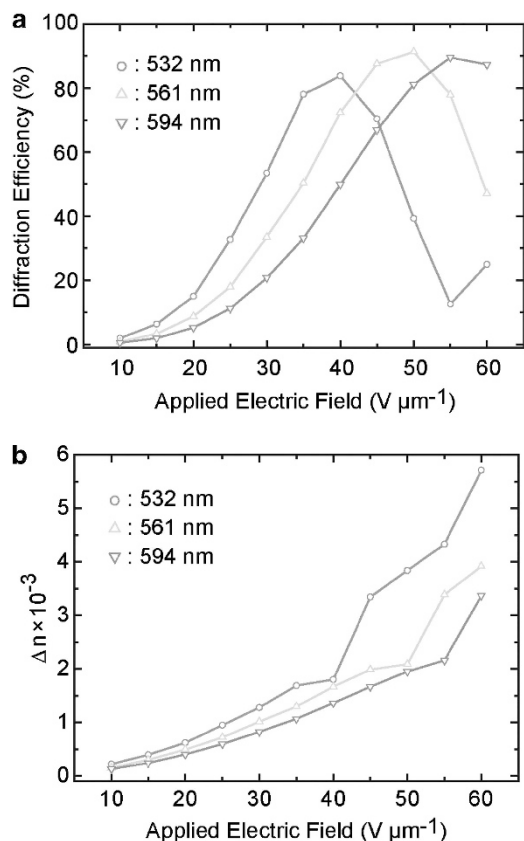


Figure 3 PR properties from DFWM. (a) Diffraction efficiency as a function of electric field. (b) Refractive index modulation as a function of electric field. Circle: 532 nm. Triangle: 561 nm. Inverse triangle: 594 nm. A full color version of this figure is available at *Polymer Journal* online.

at each operating wavelength, a larger refractive index modulation could be obtained by increasing the applied electric field. However, higher applied electric fields result in a higher risk of electrical breakdown.

A large refractive index modulation without an increased applied field is more favorable for hologram applications. Instead of using alternative materials, the goal of high diffraction efficiency at a low applied electric field may be achieved by changing the wavelength of the writing beams. A short wavelength with a strong absorption might reduce the external (absorption-loss corrected) diffraction efficiency, but increasing the internal diffraction efficiency is still useful for estimating the potential of the material for a hologram display. However, as shown in Figure 4, an intense absorption was detected at much shorter wavelengths. Thus, transparency and beam attenuation problems, which might reduce PR performance, need to be considered when the operating wavelength is chosen.

Another PR material feature to be considered is the diffraction efficiency response time. Using an applied electric field at $45 \text{ V } \mu\text{m}^{-1}$, the diffraction efficiency transient growth (Figure 5) and response times were calculated by a KWW fitting at different operating wavelengths (Table 1). Shorter wavelengths gave a faster response time, and an equilibrium state of charges trapped in the dark area was established faster when more charges were generated with time. As shown in Figure 5, transient growth of diffraction efficiency at an operating wavelength of 532 nm could not be fitted well using a single exponential function. The diffraction efficiency in this case reached a maximum value and then decreased to a steady state. This difference for 532 nm compared with the other two wavelengths is due to the change in the Δn value and the sine-squared relations between Δn and the diffraction efficiency. For the 532 nm wavelength, the Δn value was larger, and the diffraction efficiency peak as a function of applied field appeared at an applied field of $<45 \text{ V } \mu\text{m}^{-1}$, as shown in Figure 3.

The nature of the diffraction efficiency growth is originally due to the refractive index modulation growth. Due to the space-charge field formed inside the sample, the Δn value increased continuously to a saturated value, Δn_{sat} . At $45 \text{ V } \mu\text{m}^{-1}$, the Δn_{sat} for 532 nm was large, and the diffraction efficiency followed a sine-squared function of Δn (equation (4)) that reached a maximum value at a specific value of Δn that was smaller than Δn_{sat} . Then, when Δn continued increasing and reached Δn_{sat} , the diffraction efficiency would decrease to steady state after reaching the maximum value. Instead of using the diffraction efficiency, the growth of Δn was used to evaluate the response time at 532 nm. For both 561 and 594 nm, the values of Δn_{sat} were smaller

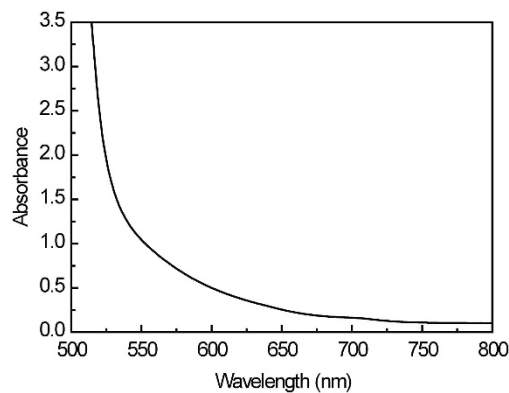
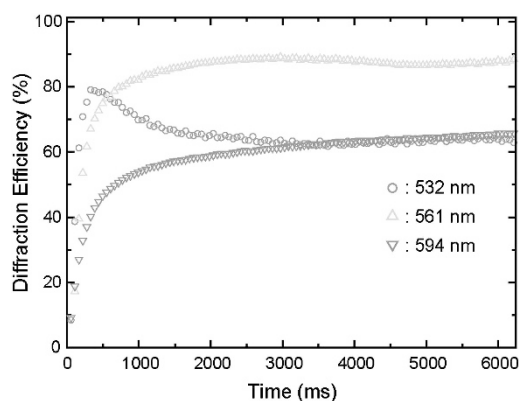


Figure 4 UV-vis absorption spectrum of PR film sample.

Table 1 Absorption coefficient, photocurrent, PR quantities and sensitivity calculated using equation (5) at different operating wavelengths

Operating wavelength (nm)	Absorption coefficient (cm^{-1})	Photocurrent ($\mu\text{A W}^{-1} \text{cm}^{-2}$) ^a	Diffraction efficiency ^b	Response time (s)/ β	Intensity (W cm^{-2})	Sensitivity ($\text{cm}^2 \text{J}^{-1}$)
532	361	1.29	0.33	0.267/ 0.8	0.172	12.5
561	210	1.04	0.18	0.28/0.8	0.174	8.7
594	129	0.95	0.11	0.452/ 0.5	0.216	3.4

Abbreviation: PR, photorefractive.

^aMeasured at $70 \text{ V } \mu\text{m}^{-1}$ ^bMeasured at $25 \text{ V } \mu\text{m}^{-1}$ **Figure 5** Time profile of diffraction response. Diffraction efficiency time profiles at 532 nm (circle), 561 nm (triangle) and 594 nm (inverse triangle). All data were measured at $45 \text{ V } \mu\text{m}^{-1}$. A full color version of this figure is available at *Polymer Journal* online.

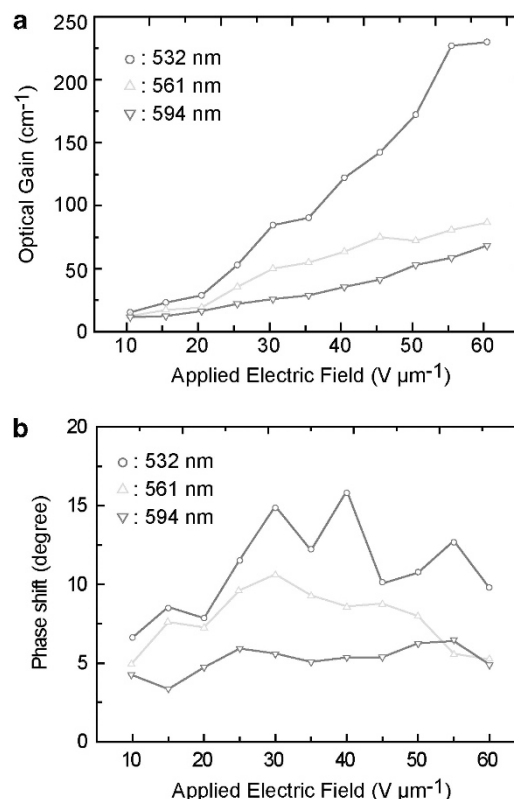
and the diffraction efficiency peak as a function of the applied field appeared at an applied field $> 45 \text{ V } \mu\text{m}^{-1}$ (Figure 3). Therefore, there was no diffraction efficiency peak in the response time curves at $45 \text{ V } \mu\text{m}^{-1}$.

The sensitivity parameter was used to choose the wavelength for the hologram display. The sensitivity is a good parameter to use to evaluate wavelength response as a function of diffraction efficiency, response time and illuminating intensity. The sensitivity is determined by diffraction efficiency, η , response time, τ , and laser intensity, I , as follows:

$$\text{Sensitivity} = \frac{\sqrt{\eta}}{I \times \tau}, \quad (5)$$

where I is the laser intensity per unit area. Table 1 summarizes the sensitivity at each wavelength. The sensitivity at 532 nm has the largest value at $12.5 \text{ cm}^2 \text{ J}^{-1}$. Thus, for the present PR composite, the 532 nm wavelength gives the best PR performance even with the lowest intensity among the three studied wavelengths (see the Materials and methods section). The results also indicated that optimizing the diffraction efficiency and response time for the hologram display could be accomplished by adjusting the operating wavelength instead of developing a new material or using harsh conditions, such as a higher applied electric field and a stronger laser intensity. Based on the obtained results, the hologram display is demonstrated under the interference beams at 532 nm (see the Dynamic hologram display section below).

One important property of a PR material is energy transfer. The space-charge field formed by a non-uniform illumination induces a

**Figure 6** PR properties from two-beam coupling. (a) Optical gain as a function of electric field. (b) Phase shift as a function of electric field. Circle: 532 nm. Triangle: 561 nm. Inverse triangle: 594 nm. A full color version of this figure is available at *Polymer Journal* online.

refractive index grating. The grating is shifted by a spatial angle, Φ , compared with the optical interference pattern. This nonlocal grating leads to an energy transfer between the two beams.⁹ For the measurement technique, p -polarization beams were used as the writing beams, because it is easier to observe the effect. The energy transfer for p -polarization beams is significantly higher than for s -polarization.²⁴ The direction of applied electric field was adjusted to reduce beam fanning. Phase-shift values were calculated using the coupled-wave theory.^{6,7,25} The results of the optical gain and phase-shift values were plotted as a function of the electric field, as shown in Figure 6. Figure 6a shows that the optical gain is larger for a 532-nm laser than for 561- and 594-nm lasers. The optical gain value using the writing beams at 532 nm is 229 cm^{-1} at $60 \text{ V } \mu\text{m}^{-1}$. This result is comparable to some high performance PR materials in the review

articles by Ostroverkhova *et al.*⁹ and Köber *et al.*¹ The large energy transfer and the phase shift detected in the two-beam coupling measurement are clear evidence indicating that the formed grating is strongly nonlocal and that the phenomenon is a fingerprint for the PR effect. The present study is focused on the application to dynamic hologram displays, thus the energy transfer is not discussed further here.

Dynamic hologram display

One fantastic application of PR materials is their use as hologram displays. The composite is potentially useful in a holographic 3D display because of the high diffraction efficiency and the ability to fabricate large samples. Following the success of material design, we built two display systems in which the hologram was clearly observed through the sample under normal light.

The system setup, shown in Figure 7a, has a typical geometry for simultaneously recording and reconstructing a hologram of a real object, which is a coin in this case. The beam from the laser source at 532 nm (300 mW, Spectra Physics, Santa Clara, CA, USA) was split off by a polarized beam splitter (PBS). The *s*-polarized beam that was

spread out with the beam expander illuminated the object. Another expanded *s*-polarized beam was directed to interfere with the reflected beam from the object on the PR sample film. A *p*-polarized expanded beam at 642 nm from a semiconductor laser source (140 mW, Omicron Laserage, Rodgau-Dudenhofen, Germany) was used as the reading beam. Figure 8a shows the photograph of the PR device before and after applying the electric field. By applying a moderate electric field of $35 \text{ V } \mu\text{m}^{-1}$, a clear hologram of the coin was successfully reconstructed. After applying the field, the hologram appeared within 1 s, and it took the same time to disappear when the applied voltage was off. This setup is simple and easy to reproduce. Thus, a hologram could be recorded and erased within a very short time using our new PR device.

We then designed a new setup using a spatial light modulator (SLM, 1920 × 1200 Holoeye LCR-1080, Berlin-Adlershof, Germany) to modulate the light as the object beam. A schematic of the setup is shown in Figure 7b. This setup provides a better observation of the dynamic properties of the PR sample. Images of the real object were captured by a CMOS camera (2 M pixels, 40 fps, Trinity Inc., Ota, Gunma, Japan) equipped with a Nikon lens. The captured images

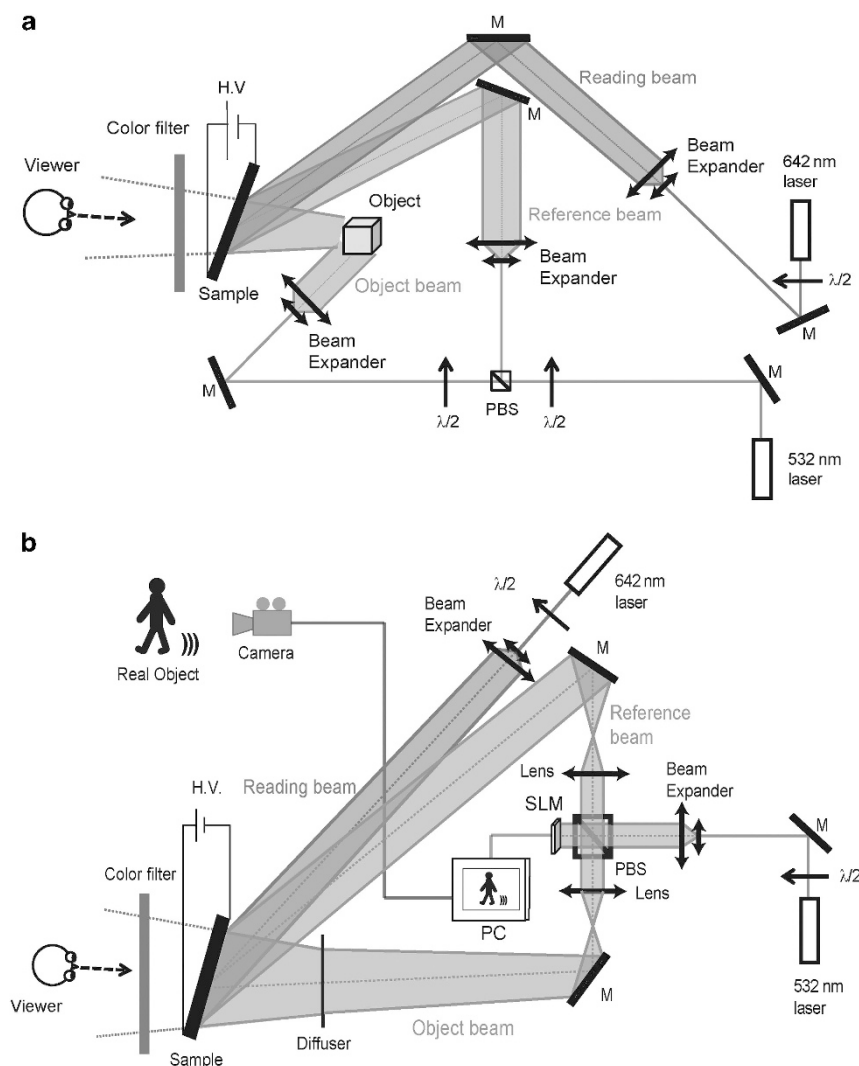


Figure 7 Experimental setup for dynamic hologram display system. (a) Reflected beam from a real object that is used as the object beam. (b) Light modulated by a SLM that is used as an object beam. For both, the writing beams are at 532 nm, and the reading beam is at 642 nm. A full color version of this figure is available at *Polymer Journal* online.

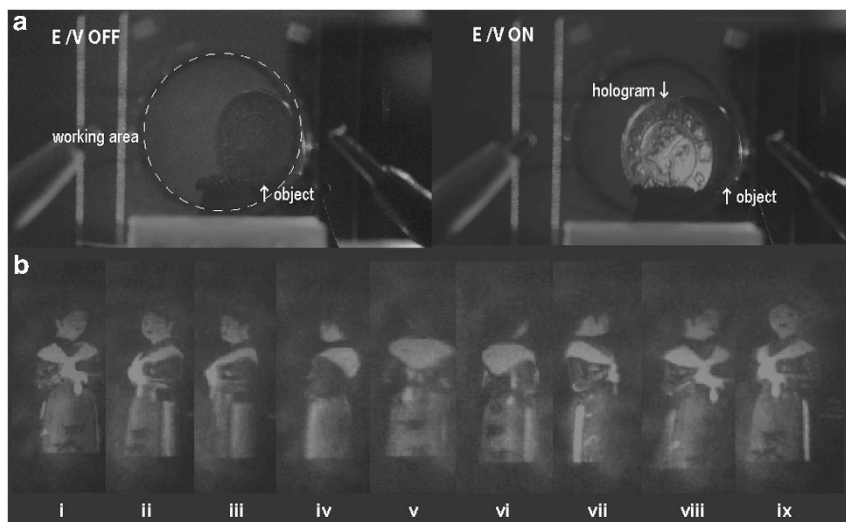


Figure 8 Hologram images in PDAA PR device. (a) Hologram of a coin. The applied field is $35\text{ V}\mu\text{m}^{-1}$. (b) Snap shots of a dynamic hologram. The applied field is $25\text{ V}\mu\text{m}^{-1}$. Supplementary Movie 1 shows a real-time dynamic hologram of a rotating doll object as observed through the PR device. A full color version of this figure is available at *Polymer Journal* online.

were continuously sent to a SLM. The laser source (532 nm) was expanded using a combination of an objective lens ($\times 10$) and a plano-convex lens and was then directed to a PBS. The *s*-polarized beam that was split off by the PBS and expanded by a lens worked as the reference beam. A *p*-polarized beam that was transmitted through the PBS was reflected on a SLM and returned to the PBS. The polarization of the reflected beam from the SLM changed to *s*-polarization. The reflected *s*-polarized beam with the object image was sent back to the PBS, split off and was directed to a plano-convex lens to create the focusing images on a diffuser. Light then passed through a diffuser that served as an object beam.

The hologram was reconstructed from the interfered pattern by a reading beam at 642 nm simultaneously with the recording process. A red color filter was used to restrain the writing beam passing through the PR device. The dynamic hologram was continuously reconstructed and watched through the PR device by naked eyes in real time. Figure 8b presents several hologram image snapshots of a doll object that was slowly rotated at a speed of 0.042 rad s^{-1} , as captured by the CMOS camera in real time. Supplementary Movie 1 shows a real-time hologram of the rotating doll object as observed through the PR device. The video demonstrates that the dynamic hologram was successfully reconstructed and smoothly followed the rotation speed of the object even at the low applied electric field ($25\text{ V}\mu\text{m}^{-1}$). The response speed is still far from video rate, but the present demonstration provides great potential for this material to be applied to real-time 3D holographic display systems operating at a low intensity and at a low electric field.

CONCLUSIONS

The PDAA polymer has been successfully applied to a PR composite with the following advantages: high photoconductivity of the triphenylamine moiety, low glass transition temperature, and a simple synthetic method. Using the PDAA matrix, large PR samples were prepared for hologram recording without using high pressure or special equipment. The PDAA-based devices were operated at a relatively low total intensity and achieved a high diffraction efficiency ($>80\%$) at a moderately applied electric field. At shorter wavelengths, the PDAA composite exhibited a larger refractive index modulation at a lower electric field, and a faster response time was obtained.

We demonstrated that PR performance can be optimized for a hologram display by changing the operating wavelength instead of increasing the applied electric field or laser intensity. By combining a good composite with the PDAA photoconductor matrix at the optimized 532 nm wavelength, we demonstrated the appearance of a dynamic hologram through the large PDAA PR device in real time. The dynamic hologram appeared even at a low electric field of $25\text{ V}\mu\text{m}^{-1}$ and without a focusing beam to increase the intensity.

ACKNOWLEDGEMENTS

This work was supported by the program for Strategic Promotion of Innovative Research and Development (SPIRE), Japan Science and Technology Agency (JST), Japan.

- 1 Köber, S., Salvador, M. & Meerholz, K. Organic photorefractive materials and applications. *Adv. Mater.* **23**, 4725–4763 (2011).
- 2 Meerholz, K., Volodin, B. L., Sandalphon, Kippelen, B. & Peyghambarian, N. A photorefractive polymer with high optical gain and diffraction efficiency near 100%. *Nature* **371**, 497–500 (1994).
- 3 Bittner, R., Bräuchle, C. & Meerholz, K. Influence of the glass-transition temperature and the chromophore content on the grating buildup dynamics of poly(N-vinylcarbazole)-based photorefractive polymers. *Appl. Opt.* **37**, 2843–2851 (1998).
- 4 Díaz-García, M. A., Wright, D., Casperson, J. D., Smith, B., Glazer, E., Moerner, W. E., Sukhomlinova, L. I. & Twieg, R. J. Photorefractive properties of poly(N-vinyl carbazole)-based composites for high-speed applications. *Chem. Mater.* **11**, 1784–1791 (1999).
- 5 Ostroverkhova, O. & Singer, K. D. Space-charge dynamics in photorefractive polymers. *J. Appl. Phys.* **92**, 1727–1743 (2002).
- 6 Tsutsumi, N. & Kasaba, H. Effect of molecular weight of poly(N-vinyl carbazole) on photorefractive performances. *J. Appl. Phys.* **104**, 073102 (2008).
- 7 Tsutsumi, N., Dohi, A., Nonomura, A. & Sakai, W. Enhanced performance of photorefractive poly(N-vinyl carbazole) composites. *J. Polym. Sci. Pol. Phys.* **49**, 414–420 (2011).
- 8 Moerner, W. E., Silence, S. M., Hache, F. & Bjorklund, G. C. Orientationally enhanced photorefractive effect in polymers. *J. Opt. Soc. Am. B* **11**, 320–330 (1994).
- 9 Ostroverkhova, O. & Moerner, W. E. Organic photorefractives: mechanisms, materials, and applications. *Chem. Rev.* **104**, 3267–3314 (2004).
- 10 Engels, C., Van Steenwinkel, D., Hendrickx, E., Schaerlaekens, M., Persoons, A. & Samyn, C. Efficient fully functionalized photorefractive polymethacrylates with infrared sensitivity and different spacer lengths. *J. Mater. Chem.* **12**, 951–957 (2002).
- 11 Herlocker, J. A., Fuentes-Hernandez, C., Ferrio, K. B., Hendrickx, E., Blanche, P. A., Peyghambarian, N., Kippelen, B., Zhang, Y., Wang, J. F. & Marder, S. R. Stabilization of the response time in photorefractive polymers. *Appl. Phys. Lett.* **77**, 2292–2294 (2000).
- 12 Iwan, A. & Sek, D. Polymers with triphenylamine units: photonic and electroactive materials. *Prog. Polym. Sci.* **36**, 1277–1325 (2011).

- 13 Blanche, P. A., Tay, S., Voorakaranam, R., Saint-Hilaire, P., Christenson, C., Gu, T., Lin, W., Flores, D., Wang, P., Yamamoto, M., Thomas, J., Norwood, R. A. & Peyghambarian, N. An updatable holographic display for 3D visualization. *J. Disp. Technol.* **4**, 424–430 (2008).
- 14 Blanche, P. A., Bablumian, A., Voorakaranam, R., Christenson, C., Lin, W., Gu, T., Flores, D., Wang, P., Hsieh, W. Y., Kathaperumal, M., Rachwal, B., Siddiqui, O., Thomas, J., Norwood, R. A., Yamamoto, M. & Peyghambarian, N. Holographic three-dimensional telepresence using large-area photorefractive polymer. *Nature* **468**, 80–83 (2010).
- 15 Thomas, J., Christenson, C. W., Blanche, P.-A., Yamamoto, M., Norwood, R. A. & Peyghambarian, N. Photoconducting polymers for photorefractive 3D display applications. *Chem. Mater.* **23**, 416–429 (2010).
- 16 Eralp, M., Thomas, J., Tay, S., Li, G., Schulzgen, A., Norwood, R. A., Yamamoto, M. & Peyghambarian, N. Submillisecond response of a photorefractive polymer under single nanosecond pulse exposure. *Appl. Phys. Lett.* **89**, 114105–3 (2006).
- 17 Tsujimura, S., Kinashi, K., Sakai, W. & Tsutsumi, N. High-speed photorefractive response capability in triphenylamine polymer-based composites. *Appl. Phys. Expr.* **5**, 064101 (2012).
- 18 Hsu, J.-C., Chen, Y., Kakuchi, T. & Chen, W.-C. Synthesis of linear and star-shaped poly[4-(diphenylamino)benzyl methacrylate]s by group transfer polymerization and their electrical memory device applications. *Macromolecules* **44**, 5168–5177 (2011).
- 19 Fehervari, A. F., Kagumba, L. C., Hadjikyriacou, S., Chen, F. & Gaudiana, R. A. Photoluminescence and excimer emission of functional groups in light-emitting polymers. *J. Appl. Polym. Sci.* **87**, 1634–1645 (2003).
- 20 Meerholz, K., De Nardin, Y., Bittner, R., Wortmann, R. & Wurthner, F. Improved performance of photorefractive polymers based on merocyanine dyes in a polar matrix. *Appl. Phys. Lett.* **73**, 4–6 (1998).
- 21 Thomas, J., Fuentes-Hernandez, C., Yamamoto, M., Cammack, K., Matsumoto, K., Walker, G. A., Barlow, S., Kippelen, B., Meredith, G., Marder, S. R. & Peyghambarian, N. Bistriarylamine polymer-based composites for photorefractive applications. *Adv. Mater.* **16**, 2032–2036 (2004).
- 22 Giang, H. N., Kinashi, K., Sakai, W. & Tsutsumi, N. Photorefractive composite based on a monolithic polymer. *Macromol. Chem. Phys.* **213**, 982–988 (2012).
- 23 Kogelnik, H. Coupled wave theory for thick hologram gratings. *Bell Syst. Tech. J.* **48**, 2909–2947 (1969).
- 24 Schloter, S., Hofmann, U., Stroehriegl, P., Schmidt, H. W. & Haarer, D. High-performance polysiloxane-based photorefractive polymers with nonlinear optical azo, stilbene, and tolane chromophores. *J. Opt. Soc. Am. B* **15**, 2473–2475 (1998).
- 25 Tsutsumi, N. & Miyazaki, W. Photorefractive performance of polycarbazolethylacrylate composites with photoconductive plasticizer. *J. Appl. Phys.* **106**, 083113 (2009).

Supplementary Information accompanies the paper on Polymer Journal website (<http://www.nature.com/pj>)